SYNTHESIS OF TiO_2 NANOPARTICLES AND CHARACTERIZATION OF Sn-3.0Ag-0.5Cu/TiO_2 VIA NANOINDENTATION AND SELECTIVE ELECTROCHEMICAL ETCHING

MUHAMAD ZAMRI BIN YAHAYA@KAMALUDDIN

UNIVERSITI SAINS MALAYSIA

2018

SYNTHESIS OF TiO_2 NANOPARTICLES AND CHARACTERIZATION OF Sn-3.0Ag-0.5Cu/TiO_2 VIA NANOINDENTATION AND SELECTIVE ELECTROCHEMICAL ETCHING

by

MUHAMAD ZAMRI BIN YAHAYA@KAMALUDDIN

Thesis submitted in fulfillment of the

requirements for the degree of

Doctor of Philosophy

April 2018

ACKNOWLEDGEMENT

Highest of gratitude to Allah SWT for His blessings in which this thesis was successfully completed. This journey had allowed me to encountered numbers of people whom contributed to this thesis in various ways. It is my honor, to convey my gratitude to those great people in my acknowledgement. First and foremost, I would like to express my deepest appreciation to my supervisor, Assoc. Prof. Dr. Ahmad Azmin Bin Mohamad for his countless guidance and support throughout this project. This follows with my co-supervisor, Prof. Dr. Mohd Zulkifly Bin Abdullah. I indeed could not wish for much supportive supervisors other than both of them. I also dedicate my acknowledgement to the Ministry of Higher Education for the awarded MyBrain15 scholarship which fulfills my financial needs. I am truly blessed to be part of the battery and solder research group, in which I was surrounded by such friendly and supportive colleagues. I am grateful for the experience and knowledge I had learned from all of these great people.

My thank also goes to the School of Material and Mineral Resources Engineering, especially to the dean and the management team for providing the excellent facilities along my studies. The support I received from the laboratories, offices and all of the staffs were most helpful and I am thankful for such cooperation. Again, I wish millions of thank you to all the people responsible to the realization of this thesis, as well as expressing my apology to whose I could not mention personally one by one. Last but not least, special thanks to my mother, Zaharah Binti Mohd Tahir and my beloved wife, Nor Zakiah Binti Yahaya for their never ending support and prayers.

Muhamad Zamri Yahaya

April 2018

TABLE OF CONTENTS

		Page
ACKNOWLEDGEMENT		ii
TABLE OF CONTENTS		iii
LIST OF TABLES		viii
LIST OF FIGURES		ix
LIST OF ABBREVIATIONS		xvi
ABSTRAK		xix
ABSTRACT		xx
CHAPTER ONE: INTRODUCTION		
1.1	Background	1
1.2	Problem statement	3
1.3	Objectives	5
1.4	Thesis outline	5
CHAPTER TWO: LITERATURE REVIEW		
2.1	Introduction	7
2.2	Lead-free solder alloy	7
2.2.1	The development of lead-free solder alloy	8
2.2.2	Composite lead-free solder alloy	9
2.3	Titanium dioxide nanoparticle as reinforcement material	9
2.3.1	Synthesis by the sol-gel method	10
2.3.2	Thermal behavior	12
2.3.3	Phase and structural analysis	15

2.3.4 Rietveld refinement 18

2.3.5 Morphological and elemental analysis 22

2.3.6 Particle size measurement 31

2.4 The Sn-Ag-Cu composite solder 33

2.4.1 Producing the Sn-Ag-Cu composite solder 34

2.4.2 The reflow profiles 35

2.4.3 Phase identification 36

2.4.4 Morphologies of the Sn-Ag-Cu composite solder 38

2.5 Hardness of the Sn-Ag-Cu composite solder 42

2.5.1 The nanoindentation test 42

2.5.2 Hardness evaluations and analysis 44

2.6 Selective etching of Sn-Ag-Cu solder alloy 48

2.6.1 Electrochemical setup and configuration 48

2.6.2 The cyclic voltammetry analysis 49

2.6.3 Selective electrochemical etching by chronoamperometry 51

2.6.4 Morphologies of the etched Sn-Ag-Cu solder alloy 52

2.6.5 The Sn removal calculation 54

CHAPTER THREE: METHODOLOGY

3.1 Introduction 56

3.2 Experimental materials 58

3.3 Preparation of TiO_2 nanoparticles 59

3.4 Characterization of TiO_2 nanoparticles 61

3.4.1 Thermal analyis 62

3.4.2 Phase and structural analysis 62

3.4.3 Rietveld refinements 62

3.4.4 Morphological, elemental and size analysis 63

3.5 Preparation of the Sn-Ag-Cu-TiO_2 composite solder 63

3.6 Characterization of the Sn-Ag-Cu-TiO_2 composite solder 66

3.6.1 The phase identification 67

3.6.2 Morphological observation 67

3.6.3 Hardness measurment and evaluation 67

3.7 Preparation of the Sn-Ag-Cu-TiO_2 composite solder electrode for selective electrochemical etching 69

3.8 Characterization of the selectively etched Sn-Ag-Cu-TiO_2 composite solder 70

3.8.1 The electrochemical evaluations 71

3.8.2 Phase analysis 72

3.8.3 Morphological and elemental evaluation 72

3.8.4 The mass and volume removal calculation 73

CHAPTER FOUR: SOL-GEL SYNTHESIS OF TiO_2 NANOPARTICLE BY STORAGE AND CENTRIFUGE PRECIPITATION

4.1 Introduction 74

4.2 The thermal analysis 74

4.3 Phase and structural analysis 77

4.4 Rietveld refinement analysis 80

4.5 Morphology and elemental characterization 89

4.6 Particles size determination 96

4.7 Mechanism of the centrifuge and storage precipitation 98

4.8 Summary 102

CHAPTER FIVE: CHARACTERIZATION OF THE Sn-Ag-Cu-TiO_2 COMPOSITE SOLDER BY NANOINDENTATION

5.1 Introduction 103

5.2 Morphologies of the SAC305 composite solders analysis 103

5.3 The phase identification 110

5.4 Depth displacement and hardness analysis 112

5.5 Mechanism on the hardness improvement for the composite solders 121

5.6 Summary 124

CHAPTER SIX: SELECTIVE ELECTROCHEMICAL ETCHING OF THE Sn-Ag-Cu-TiO_2 COMPOSITE SOLDER

6.1 Introduction 125

6.2 Electrochemical behavior of the Sn-Ag-Cu-TiO_2 composite solder 125

6.3 The selective electrochemical etching 128

6.4 Phase analysis 130

6.5 Morphologies of the etched Sn-Ag-Cu-TiO_2 composite solder 133

6.6 Distribution of the TiO_2 nanoparticles reinforcement 141

6.7 The Sn removal calculation 144

6.8 Mechanism of the etched Sn-Ag-Cu-TiO_2 composite solder 147

6.9 Summary 151

CHAPTER SEVEN: CONCLUSIONS AND RECOMMENDATIONS

7.1 Conclusions 152

7.2 Recommendations for future works 154

REFERENCES 157

APPENDICES

LIST OF PUBLICATIONS

LIST OF TABLES

		Page
Table 2.1	Structural and microstructural data obtained after Rietveld refinement for TiO_2 nanoparticles synthesized with varying precursor to solvent ratio [66]	20
Table 2.2	Crystallographic data and results of Rietveld refinement of nanocrystalline TiO_2 anatase and brookite [82]	22
Table 3.1	The list of materials used in this work	58
Table 3.2	The equipment involved in this work	58
Table 3.3	Calcine temperatures with respect to the precipitation conditions for 2 hours of calcination	61
Table 3.4	TiO_2 nanoparticles weight percentage with respect to the prepared SAC305 composite solders	64
Table 3.5	TiO_2 nanoparticles weight percentage with respect to the prepared SAC305 composite solders	72
Table 4.1	Quantitative analysis of the TiO_2 nanoparticles through the Rietveld refinement method	86
Table 5.1	Hardness evaluation on the SAC305 and SAC305 composite solders by the nanoindentation	119
Table 6.1	The calculated mass and volume for the removed Sn from electrochemical etching of the pure and composite SAC305	146

LIST OF FIGURES

		Page
Figure 2.1	Schematic representation of the sol-gel processing by various synthesis route [52]	12
Figure 2.2	The TGA curves of the synthesized TiO2 nanoparticles with different NH_4Cl ratio of (a) R = 1, (b) R = 2 and (c) R = 0 [54]	13
Figure 2.3	The TGA curves for the sol-gel synthesized TiO_2 nanoparticles with different amount of added acetic acid [56]	14
Figure 2.4	X-ray diffraction patterns of the as-dried TiO_2 precursor samples calcined at different temperatures in air for 2h [71]	16
Figure 2.5	The XRD patterns of calcined TiO_2-based photocatalysts with different Fe^{3+} doping levels doping levels [67]	17
Figure 1.6	The refined XRD patterns of the TiO_2 nanoparticles synthesized with varying ratio of precursor to solvent [82]	19
Figure 2.7	The fitted profiles of calcined TiO_2-based photocatalysts with different Fe^{3+} doping concentration [83]	21
Figure 2.8	SEM images of amorphous TiO_2 after heat treatment at different temperatures: (a) without heat treatment; (b) 450°C; (c) 700°C and (d) 900°C [84]	24
Figure 2.9	SEM micrograph of powder annealed at (a) 600 °C, (b) 700 °C, (c) 800 °C and (d) 900 °C [87]	25
Figure 2.10	Micrographs of the TiO_2 nanoparticles obtained by (a) HRTEM and (b) lattice fringes measurement [67]	27

Figure 2.11	TEM images of (a) TiO_2 without cellophane membrane and calcined at 400 °C for 3 h, (b) TiO_2 with cellophane membrane and calcined at 400 °C, (c) 500 °C and (d) 600 °C for 3 h and (e) lattice fringe image of (b) [93]	28
Figure 2.12	EDX spectrum of the TiO_2 nanoparticles, obtained after calcining at (a) 400 °C (b) 700 °C and (c) 1000 °C temperature under N_2 atmosphere [97]	30
Figure 2.13	SEM images of as-prepared TiO_2 nanoparticles (a) without heat treatment and (b) with heat treatment at 600 °C for 3 h in air, as well as the corresponding particle size distribution histograms drawn at right [100]	32
Figure 2.14	TEM micrographs and size distribution histograms of TiO_2 nanoparticles synthesized from (a–c) TBOT, (d-f) adding 1 mL acetic acid (d–f), and (g–i) synthesized from TTIP with 1 mL acetic acid [71]	33
Figure 2.15	Reflow profile of the SAC-TiO_2 composite solder alloy on Ni-P coated Cu substrate [122]	36
Figure 2.16	X-ray diffraction spectrum of the SAC solders with the addition of different amounts of TiO_2 nano-powders [20]	37
Figure 2.17	X-ray diffraction scans of composite solder matrix for the Sn–3.0Ag–0.5Cu–0.6TiO2 solder joint [23]	38
Figure 2.18	SEM micrographs of as-cast solders: (a) SAC, (b) SAC-0.25TiO_2, (c) SAC-0.5TiO_2 and (d) SAC-1TiO_2 [20]	39
Figure 2.19	SEM micrographs of cross-sectional view of the interfaces between Sn–3.0Ag–0.5Cu–xTiO2 and Cu substrate reflowed for 90 s: a x = 0; b x = 0.05; c x = 0.1; and d x = 0.6 wt% [17]	40

Figure 2.20	Micrograph and EDX spectrum for Sn–3.0Ag–0.5Cu–0.1TiO_2 solder joints: (a) micrograph of interface, (b-c) EDX spectrum for box in (a) [23]	41
Figure 2.21	(a) Indentation mark on the SAC305-diamond composite solder and (b) average hardness versus the amount of added diamond nanoparticles [111]	46
Figure 2.22	Microstructures of as-prepared solder alloys: (a) Sn58Bi0.7Zn, (b) Sn58Bi0.7Zn0.038GNS, (c) Sn58Bi0.7Zn0.076GNS, (d) Sn58Bi0.7Zn0.114GNS and (e) load-depth curves obtained from nanoindentation [148]	47
Figure 2.23	CV curves of Sn–Cu, Sn–Ag and Sn–Ag–Cu electrodeposited from weakly acidic baths [159]	50
Figure 2.24	The CA curve for the electrochemical etching of Sn removal with 30 and 120 s etching time [162]	52
Figure 2.25	SEM images of the SAC joints (a) un-etched samples, (b) chemically etched for 7 days and (c) electrochemically etched for 120 s [16, 156]	53
Figure 2.26	SEM images and EDS mapping of solder joints created with VPS techniques at the matrix and Cu–Sn interface [156]	54
Figure 2.27	The calculated volume of the removed Sn phase with respect to different selective electrochemical etching durations [157]	55
Figure 3.1	Overall flowchart on the experimental work	57
Figure 3.2	The milky TiO_2 nanoparticles solution	59
Figure 3.3	The final TiO_2 nanoparticles product after grinding	60
Figure 3.3	The SAC305-TiO_2 solder paste obtained at different ball milling configurations	64
Figure 3.4	Custom aluminum stencil for solder paste printing	65
Figure 3.5	The temperature profile used for solder paste reflowing	66

Figure 3.6	Schematic of the indentation path by the nanoindentation measurement for hardness evaluation	68
Figure 3.8	The prepared working electrode used in the electrochemical evaluations	70
Figure 3.9	The actual and schematic of the electrochemical setups for the CV and CA	71
Figure 4.1	TGA curves of the TiO_2 nanoparticles synthesized by centrifuge and storage conditions in air atmosphere (the shaded area represents the temperature range for crystalline TiO_2 nanoparticles)	76
Figure 4.2	X-ray diffraction patterns of TiO_2 nanoparticles at various calcination temperatures synthesized through centrifuge (the shaded area represents changes on the anatase and rutile peak)	78
Figure 4.3	X-ray diffraction patterns of TiO_2 nanoparticles at various calcination temperatures synthesized through storage (the shaded area represents changes on the anatase and rutile peak)	80
Figure 4.4	Anatase percentage and crystallite size of the TiO_2 nanoparticles as a function of calcine temperatures	82
Figure 4.5	Weighted R profile and GOF of the TiO_2 nanoparticles as a function of calcine temperatures	84
Figure 4.6	Crystallographic representation of the C500 TiO_2 nanoparticles simulated by CASTEP (a) ball and stick configuration and (b) polyhedron configuration	88
Figure 4.7	SEM images of the TiO_2 nanoparticles synthesized by the sol-gel centrifuge method with corresponding EDX pattern for (a) as synthesized, (b) C100, (c) C200 and (d) C300	90

Figure 4.8	SEM images of the TiO_2 nanoparticles synthesized by the sol-gel centrifuge method with corresponding EDX pattern for (a) C400, (b) C500, (c) C600 and (d) C700	91
Figure 4.9	Higher magnification SEM images of the C500 TiO_2 nanoparticles with corresponding EDX pattern	92
Figure 4.10	SEM images of the TiO_2 nanoparticles synthesized by the sol-gel storage method with corresponding EDX pattern for (a) as synthesized, (b) S100, (c) S200, and (d) S300	94
Figure 4.11	SEM images of the TiO_2 nanoparticles synthesized by the sol-gel storage method with corresponding EDX pattern for (a) S400, (b) S500, (c) S600, and (d) S700	95
Figure 4.12	TEM and HRTEM images of C500 TiO_2 nanoparticles at magnification of (a) 97 kx, (b) 195 kx, (c) 610 kx and (d) magnified image of selected square in (c)	97
Figure 4.13	Particle size distribution of C500 TiO_2 nanoparticles	98
Figure 4.14	Proposed mechanism of the formation of TiO_2 nanoparticles synthesized through (a) centrifuge and (b) storage conditions	101
Figure 5.1	Micrograph of the cross-sectioned matrix for (a) SAC305, (b) SAC305-0.25T, (c) SAC305-0.50T, (d) SAC305-1.00T, (e) SAC305-1.50T, (f) porosity in SAC305-1.50T and EDX scan (g) area in (a) and (h) area in (b)	105
Figure 5.2	Micrograph of the cross-sectioned IMC layer for (a) SAC305, (b) SAC305-0.25T, (c) SAC305-0.50T, (d) SAC305-1.00T (e) SAC305-1.50T and (f) EDX pattern; red box in (d) represent the area scan	109

Figure 5.3	The XRD pattern of the anatase TiO_2, pure and composite SAC305 solder	112
Figure 5.4	Areas of the nanoindentation marks on the cross-sectioned surface of the (a) SAC305, (b) SAC305-0.25T, (c) SAC305-0.50T, (d) SAC305-1.00T and (e) SAC305-1.50T	114
Figure 5.5	Hysteresis plot of the loading and unloading indenter for (a) SAC305, (b) SAC305-0.25T, (c) SAC305-0.50T, (d) SAC305-1.00T and (e) SAC305-1.50T	115
Figure 5.6	Comparison on the average hardness values from the nanoindentation points along the measurement path for the SAC305 and SAC305 composite solders	117
Figure 5.7	The established hardness profile from the nanoindentation points along the measurement path for the SAC305 and SAC305 composite solders	120
Figure 5.8	Proposed mechanism on the hardness improvement corresponding to the (a) larger and (b) smaller IMC phases	123
Figure 6.1	CV curves for the pure and composite SAC305 solder alloy	126
Figure 6.2	CA curves for the pure SAC305 solder alloy	129
Figure 6.3	CA curves for the composite SAC305 solder alloy	129
Figure 6.4	The XRD pattern of the selectively etched pure SAC305 solders	132
Figure 6.5	The XRD pattern of the selectively etched composite SAC305 solders	132
Figure 6.6	Micrograph of the selectively etched P30, P60, P90, P120, P150 and the EDX pattern of the point scan marked in P120	135
Figure 6.7	Micrograph of the selectively etched C30, C60, C90, C120, C150 and the EDX pattern of the point scan marked in C150	136

Figure 6.8	Micrograph on the IMC layer for the selectively etched P30, P60, P90, P120, P150 and the EDX pattern of the point scan marked in P150	139
Figure 6.9	Micrograph on the IMC layer for the selectively etched C30, C60, C90, C120 and C150	140
Figure 6.10	Micrographs of the (a) selectively etched C120, (b) magnification images indicated by the red box in (a), (c) magnification images indicated by the yellow box in (a), (d) EDX spectra of the point scan marked in (b) and (e) EDX spectra of the point scan marked in (c)	143
Figure 6.11	The calculated mass and volume of the removed β-Sn for the pure and composite SAC305	145
Figure 6.12	Schematic on the mechanism of the selective electrochemical etching for the pure SAC305	148
Figure 6.13	Schematic on the mechanism of the selective electrochemical etching for the composite SAC305 incorporated with the TiO_2 nanoparticles	150

LIST OF ABBREVIATIONS

Pb	Lead
Sn	Tin
Ag	Silver
Cu	Copper
Sb	Antimony
Ni	Nickel
Ga	Galium
Fe	Iron
Zr	Zirconium
Ti	Titanium
O	Oxygen
Sn-In	Tin-indium
Sn-Ag	Tin-silver
Sn-Bi	Tin-bismuth
Sn-Zn	Tin-zinc
Sn-Zn-In	Tin-zinc-indium
Sn-Bi-Zn	Tin-bismuth-zinc
Sn-Ag-Cu	Tin-silver-copper
SAC	Sn-Ag-Cu
SAC305	Sn-3.0Ag-0.5Cu
Al_2O_3	Aluminum oxide
Fe_2NiO_4	Iron nickel oxide
ZrO_2	Zirconium dioxide

TiO_2	Titanium dioxide
GNS	Graphene nanosheets
IMC	Intermetallic compounds
$Ti(OBu)_4$	Titanium (IV) butoxide
$TiCl_3$	Titanium (III) chloride
$TiCl_4$	Titanium (IV) chloride
$TiBr_4$	Titanium (IV) tetrabromide
TTIP	Titanium (IV) isopropaxide
TGA	Thermogravimetric analysis
XRD	X-ray diffraction
ICSD	Inorganic crystal structure database
GOF	Goodness of fit
R_{wp}	Weighted R Profile
R_{exp}	R expected
FESEM	Field emission scanning electron microscope
HRTEM	High resolution transmission electron microscope
SE	Secondary electron
EDX	Energy dispersive X-ray
HV	Hardness Vickers
HB	Hardness Brinell
CSM	Continuous stiffness measurement
CV	Cyclic voltammetry
CA	Chronoamperometry
CE	Counter electrode
SCE	Saturated calomel electrode

WE	Working electrode
N_2	Nitrogen
H_2SO_4	Sulfuric acid
SO_4^{2-}	Sulfate ion
CO_2	Carbon dioxide
Q	Charge
m	Mass
M	Molar mass
F	Faraday’s constant
V	Volume

SINTESIS NANOPARTIKEL TIO_2 DAN PERINCIAN Sn-3.0Ag-0.5Cu/TiO_2 MELALUI KAEDAH LEKUKAN NANO DAN PUNARAN ELEKTROKIMIA TERPILIH

ABSTRAK

Pengagihan nanopartikel TiO_2 dalam Sn-3.0Ag-0.5Cu (SAC305) telah dikaji melalui kaedah lekukan nano dan punaran elektrokimia terpilih. Saiz optimum untuk nanopartikel TiO_2 telah diperolehi melalui sintesis sol-gel dengan kaedah mendakan empar. Campuran sebati komposit SAC305-TiO_2 telah dihasilkan dengan kaedah pengisaran bebola. Penambahan peratusan berat TiO_2 telah mengubahsuai morfologi komposit SAC305-TiO_2. Penambahan TiO_2 secara berlebihan dengan 1.5 wt. % telah mengurangkan nilai kekerasan. Prestasi mekanikal yang optimum telah diperoleh oleh komposit SAC305-TiO_2 yang dimasukkan dengan 1.0 wt. % partikel penguatan. Profil kekerasan menunjukkan agihan dominan partikel TiO_2 berhampiran dengan permukaan antara pateri/substrat. Komposit SAC305-TiO_2 yang optimum menunjukkan kelakuan elektrokimia yang lebih baik melalui nilai arus yang lebih tinggi. Penambahan pada tempoh punaran telah menambahbaik proses pemerhatian pada bentuk dan saiz kompoun Cu_6Sn_5 dan Ag_3Sn. Tempoh punaran sehingga 150 s telah merosakkan struktur kompoun Cu_6Sn_5 akibat daripada pembuangan Sn secara berlebihan. Pemerhatian terhadap nanopartikel TiO_2 telah diperolehi melalui mikrograf magnifikasi tinggi pada tempoh punaran optimum 120 s. Kluster nanopartikel TiO_2 diperhatikan berhampiran kawasan lapisan kompoun Cu_6Sn_5. Nilai pengiraan jisim dan isipadu pengeluaran Sn yang lebih tinggi diperolehi oleh SAC305-TiO_2 adalah disebabkan oleh kesan perubahan morfologi yang lebih kecil.

SYNTHESIS OF TiO_2 NANOPARTICLES AND CHARACTERIZATION OF Sn-3.0Ag-0.5Cu/TiO_2 VIA NANOINDENTATION AND SELECTIVE ELECTROCHEMICAL ETCHING

ABSTRACT

Distributions of incorporated TiO_2 nanoparticles in the Sn-3.0Ag-0.5Cu (SAC305) solder alloy were investigated by nanoindentation and selective electrochemical etching. Optimum size of the TiO_2 reinforcement particles were obtained by the sol-gel centrifuge precipitation method. The SAC305-TiO_2 composite solder was successfully blended by the aid of ball milling. Increment on the TiO_2 weight percentage significantly refined the morphologies of the SAC305-TiO_2 composite solder. Excessive TiO_2 addition of 1.5 wt. % induced a reduction on the hardness value. The highest hardness performance was obtained for the SAC305-TiO_2 composite solder with 1.0 wt. % of incorporated reinforcement particles. The hardness profiles indicate the dominant distribution of the TiO_2 nanoparticles near the solder/substrate interfaces. The optimum SAC305-TiO_2 composite solder attained slightly better electrochemical behavior with higher recorded current. Increment on the etching time mainly improved the observation on the shape profile and size refinement of the Cu_6Sn_5 and Ag_3Sn IMC. Etching time up to 150 s deteriorates the morphologies of the IMC phase due to excessive removal of the Sn. Observation on the TiO_2 nanoparticles were obtained by higher magnification on the micrographs with optimum etching time of 120 s. Clusters of the TiO_2 nanoparticles were observed to cling onto the Cu_6Sn_5 IMC layer. Higher calculated mass and volume of the Sn removal were attained by the SAC305-TiO_2 composite solder due to much favorable dissolution induced by the refinement on the morphologies.

CHAPTER ONE

INTRODUCTION

1.1 Background

It can be defined that soldering is a process of creating a metallurgical bond/joint between two or more metal parts, involving the melting of a filler material which is basically the solder alloy [1]. These joints not only serve as a bridge which provides electrical connectivity, but also acts as a mechanical support-structure and heat dissipation medium which was generated by the electronic components upon operation [2]. Futhermore, ever since the banning of conventional Pb-based solders in 2006 due to the concern on toxicity issues posed by Pb, much efforts had been put in developing potential replacement candidate among Pb-free solder alloys.

As electronic devices continuously improved; bearing more features and functions, the challenges on developing high-performance Pb-free solder alloys also grows. To add, miniaturization in size for these devices requires fine-pitch interconnections (down to 10 μm) and smaller integrated circuit (IC) components [3]. A quote by Meinshausen et al. [4] in his articles stated that size reduction of electronic components (eg: transistor) had already reached its limits. In other words, this means that to add more features, there are no other ways but to incorporate more components on the circuit; which translate to more fine-pitch solder connections. These greatly influence the current and even future views of scholars in conducting lead-free solder researches which now mainly focused on the mechanical reliability of the solder joints.

Among various Pb-free solder families, the tertiary Sn-Ag-Cu (SAC) system particularly the SAC305 was the most commercially used Pb-free solder alloy in the current industries. The melting characteristic of the Sn-3.0Ag-0.5Cu (SAC305) which is comparable to the previous Pb-based solder marked the initiation for the wide application of the SAC305 solder alloy. This explains why the SAC305 had received huge interest among researchers in improving its mechanical performance. Such works includes compositional modification of the SAC305 [5], investigation on reflowing parameters [6] and effect of heat treatments [7]. However, the most implied approaches are by incorporating non-reacting reinforcement materials to produce SAC305 composite solders.

Several type of nanoparticles filler such as the Al_2O_3 [8], Fe_2NiO_4 [9], ZrO_2 [10] and TiO_2 [11] which were added into the SAC305 had produced various influence on the resultant mechanical properties. The TiO_2 specifically posed a significant potential due to its advantages in ease of production, non-toxic and relatively lower cost. For example, promising improvement up to 37% on the tensile and hardness values of the SAC305-TiO_2 composite solder were reported by Tang et al. [12] in his work. Additionally, the presence of the TiO_2 nanoparticles was found to induce grain refinement effects for the Ag_3Sn and Cu_6Sn_5 intermetallic compound (IMC) phases. The Cu_6Sn_5 IMC layer was also suppressed, avoiding excessive growth on the thickness of the layer. This is important as the solder-substrate interfaces are commonly the initial fracture point of a solder joints; thicker IMC layer will jeopardize the connection reliability [13].

Although these literature findings clearly reflect the potential of the SAC305-TiO_2 composite solder, it is expected that this performance can be further enhanced if a more detailed investigation were designed, yielding in-depth data and

understanding. Having said that, the advancement in characterization techniques together with new ideas and analysis approaches are the mainly the key to fully attain the improvement of the SAC305-TiO_2 composite solder.

1.2 Problem statement

It is clear that ultra-fine pitch interconnections are the future in soldering technologies. With it, the mechanical performances of the lead-free solders are becoming the major concern among scholars. Current approaches of producing composite solder shows great potential in achieving better mechanical reliability of solder joints. For instance, incorporation of fine nanoparticles particularly the TiO_2 were intensively studied in various lead-free solders systems, including the SAC305.

However, brief understanding on the concept of compositing indicates that smaller reinforcement particles are much preferable due to the larger surface areas. This together with the constrain in term of the fine pitch dimension in solder joint applications further supports the need of such small nanoparticles. With such small size, better distributions of the reinforcing TiO_2 nanoparticles in the SAC305 were most likely possible. Such distribution will impede larger dislocation movements and indeed improve the mechanical properties of the SAC305. This prerequisite in size narrow down the favorable TiO_2 polymorphs to the anatase phase (anatase contains smaller size than rutile or brookite) [14]. It is known that the sol-gel process can produced such ultrafine anatase TiO_2 and among the parameters, the initial precipitation conditions pose significant influences on the end particle sizes. To relate, such fine reinforcement size contains larger surface area and distribute better; favors the mechanical improvement of the SAC305.

As for the characterization of the SAC305-TiO_2 composite solders, current reports mainly lingers on series of 'standard' analyses. From the mechanical properties point of view, this analyses commonly includes the determination of the tensile and hardness values [12, 15]. In order to further tune or improve the SAC305-TiO_2 composite solders, it is highly essential to understand the distribution behavior of the TiO_2 nanoparticles in the SAC305. Much can be exploits (needs of preliminary treatment, favorable reflow condition, etc.) with such information which can allow the possibility for achieving better performance of the SAC305 solder alloys.

The highlights in discussing the mechanical improvement of SAC305-TiO_2 or even other composite solders are attributed to the microstructural refinement. These refinement of the IMC phases (due to the presence of TiO_2 nanoparticles) were reported to induce strengthening effects such as the distribution strengthening mechanisms [16]. It is noted that the incorporated TiO_2 nanoparticles are non-reacting, thus distribution are favorable on the boundaries of the IMC phases. However, clear observation on the TiO_2 distribution in the SAC305 were difficult with the usage of conventional morphological analyses from light or electron microscopy. The idea of removing certain phase particularly the Sn matrix prior to the morphological observation may resolve such issue, revealing the TiO_2 nanoparticles.

Thus, from all of the stated motivation, firstly, the effects of promoting or hindering alkyl absorbent on the amorphous TiO_2 aggregates were investigated. The approach is to compare the centrifuge (hinder) with storage (promote) precipitation in yielding ultrafine TiO_2 nanoparticles. Subsequently, the synthesized TiO_2 nanoparticles incorporated into the SAC305 were evaluated by a distinct indentation arrays from the nanoindentation. The established hardness profiles were then utilized in investigating the improvement behavior attained and to reflect the distribution of

the TiO_2 nanoparticles in the SAC305. In observing the TiO_2 nanoparticles, the electrochemical etching process were imposed to selectively removed the Sn matrix. This will improve the overall morphological analysis particularly in observing the distribution of the TiO_2 nanoparticles in the SAC305.

1.3 Objectives

The objectives of this work are to:

i. Synthesize TiO_2 nanoparticle by sol-gel centrifuge and storage precipitation routes.
ii. Evaluate and obtain the hardness profile of the Sn-3Ag-0.5Cu/TiO_2 composite solder by nanoindentation.
iii. Observe the TiO_2 nanoparticle in the Sn-3Ag-0.5Cu/TiO_2 composite solder by prelimenary selective electrochemical etching treatment.

1.4 Thesis outline

This part of the thesis provides an introduction of the research project together with the related problem statements. The objectives of the work were also presented accordingly. The subsequent Chapter 2 contains the reviews on the fundamental and current research works in synthesizing TiO_2 nanoparticles by the sol-gel method and the efforts of incorporating the TiO_2 nanoparticles as reinforcement materials in SAC305 to improve the overall end properties. The concept of selective electrochemical etching in aiding the morphological analysis of SAC305-TiO_2 composite solder was also documented.

The experimental method of this research work was discussed in Chapter 3. This includes the preparation of the TiO_2 nanoparticles, production of the SAC305-TiO_2 composite solder and conducting the selective etching. The data and analysis of the synthesized TiO_2 nanoparticles by centrifuge and storage precipitation were contained in Chapter 4. Chapter 5 presented the characterization results conducted on the prepared SAC305-TiO_2 composite solder. The hardness profiles were established and the distributions of the TiO2 nanoparticles in the SAC305 were examined. In Chapter 6, detailed morphological behavior of the SAC305-TiO_2 composite solder contributed by the selective electrochemical etching were shown and discussed. The removed mass and volume of the Sn were also calculated.

Lastly, summaries and conclusions of the entire thesis were stated in Chapter 7. This is to highlights the potential of the selective electrochemical etching in aiding the characterization of SAC305 solder alloy. Plus, gap for improvements were also suggested in conducting related future works.

CHAPTER TWO

LITERATURE REVIEW

2.1 Introduction

In this chapter, literatures on the development of the Sn-Ag-Cu (SAC) pure and composite solder alloys were presented accordingly. Reviews on the synthesis, thermal, phase, structural and morphological analysis of the commonly incorporated TiO_2 nanoparticles were discussed at the earlier part of the chapter. This then followed by the formulation of the SAC composite solder and the hardness performance currently achieved by recent scholarly works. The basic concept and process on the selective electrochemical etching of the SAC solder alloys were later introduced. Analysis on the etching performance consisting of the cyclic voltammetry, chronoamperometry, morphological and theoretical calculation analysis were included as well at the end of the chapter.

2.2 Lead-free solder alloy

Ever since 2006, the utilization of lead (Pb)-free solder in electronic packaging began to dominate the global electronic industries. This phenomenon mainly followed the environmental regulations in eliminating the usage of Pb-bearing solders due to the inherent toxicity characteristic of Pb [2]. This process however were not merely as simple as replacing the materials, but involves huge challenges in term of electronics manufacturability, adaptability and performances.

This indeed has prompted the races on the Pb-free solder development both in the industries and academic field. Although Pb was mainly removed from the

system, the Sn however was still kept as the dominant composition in most Pb-free solder alloys. Eventually, in attaining the optimum performance of the Pb-free solder, the remaining compositions were filled up by numerous metallic materials along the formulation process. As a result, various families of Pb-free solder alloy emerges into the play; such as the Sn-Bi [17], Sn-Zn [18], Sn-Cu [19], Sn-Ag [20], Sn-Zn-In [21, 22], Sn-Bi-Zn [23] and Sn-Ag-Cu [6, 24-30].

2.2.1 The development of lead-free solder alloy

The banning of Pb-based solder marked the initiation of rapid development for lead-free solder alloys. The motivation of finding a replacement material now turn into an effort which aims to obtain better performances than the previous Pb-based solder. The large characteristics which sum up the overall performance of a particular solder alloy further enlarged the scales of current and possibly future development trend for the lead-free solders.

Such characteristics for potential lead-free solders generally include the wettability behavior [31], thermal dissipation [32], solderability [29] and mechanical performances [11, 25, 33]. However, electronic devices nowadays undergo a significant size reduction mainly to cope with current market demands. This one factor infused large attention among scholars regarding the mechanical properties of the miniaturized joints. The physical behavior of the solder alloys towards deformation is crucial in maintaining the structural integrity of the interconnections [34]. Variety of approaches had been studied in improving the mechanical performance of Pb-free solders; two most common methods are mainly on the modification of the solder materials which is alloying [35] and incorporating reinforcement particles, producing composite solders [16, 36].

2.2.2 Composite lead-free solder alloy

The composite approach had gained significant preferences in current academic works involving the Pb-free solders. Solely aiming in improvising the mechanical properties of a particular material, the incorporation of fine particles into the Pb-free solder seems theoretically beneficial in attaining better mechanical characteristic and properties. This indeed had been academically proven ever since the idea was initiated in 1998 [37]. The approaches/methods itself had undergone a series of advancement throughout the years by first involving addition of microparticles [38] and now shifting to the usage of nanoparticles [25, 39, 40]. These efforts particularly involve the addition of non-reacting, non-coarsening oxide dispersoids such as, Al_2O_3 [8], Fe_2NiO_4 [9], ZrO_2 [10] and TiO_2 [11].

2.3 Titanium dioxide nanoparticle as reinforcement material

It is well known that the TiO_2 nanoparticles had drawn major interest in various research fields such as the studies in photovoltaics [41], photocatalysis [42], batteries [43], biomedical products [44] and indeed as filler materials in solder alloys [45]. Each of the stated field however demanded varying characteristic of the respected TiO_2 nanoparticles.

Merits such as low in cost, non-toxic and ease of production of the TiO_2 were mainly responsible regarding to its popularity in SAC305 studies [46]. Positive reports on the incorporation of TiO_2 nanoparticles includes the reduction on the average size (~ 5 µm) and spacing (~ 15 µm) of intermetallic compound (IMC) [47]. Plus, the IMC layer growth can also been suppressed by the addition of TiO_2 nanoparticles [31]. Mechanically, improvement of up to 34% in the hardness values had also been attained [11]. However, it is important to note that the factors

determining these end improvement are mainly dependent on the synthesis routes used to produce the TiO_2 nanoparticles. In the case of Pb-free solder application, the influences of the reinforcement particles were highly related to the size factor of the particular TiO_2 nanoparticles [8].

2.3.1 Synthesis by the sol-gel method

Ever since 1971, the sol-gel was the most significant synthesis method known and applied in producing multicomponent oxides such as the TiO_2 [48]. Parameters such as the type of precursors [49], the pH of solution [50], preliminary solution treatment [51] and calcination temperatures [52] yielded varying properties of the resultant TiO_2 nanoparticles.

In brief, the sol-gel method is the process of transformation from sols (solid particles suspended in liquid) into gels (particulate networks of sols). This mainly involves two main reaction; hydrolysis and condensation (Figure 2.1). In synthesizing TiO_2 nanoparticles, commonly used precursor includes $Ti(OBu)_4$ [53], $TiCl_3$ [49], $TiCl_4$ [54], $TiBr_4$ [55] and $Ti[OCH(CH_3)_2]_4$ (TTIP) [56]. These precursors hydrolyzed with the addition of water (hydrolysis) and form complex three-dimensional network (condensation) as the following equations,

Hydrolysis:

$$Ti(OR)_4 + 4H_2O \rightarrow 2Ti(OH)_4 + 4ROH \quad (1)$$

Condensation:

$$Ti(OH)_4 + Ti(OH)_4 \rightarrow 2TiO_2 + 4H_2O \text{ (oxolation)} \quad (2)$$

$$Ti(OH)_4 + Ti(OR)_4 \rightarrow 2TiO_2 + 4ROH \text{ (alcoxolation)} \quad (3)$$

where R in the equation represents ethyl, i-propyl, n-butyl and etc [57, 58]. The titanium precursor is often diluted prior to the addition of water. This can reduce the rapid reaction rate of the hydrolysis process.

Size and morphology of the end TiO_2 nanoparticles are highly influenced by the precursor-water ratio. Lower ratio of water-precursor resulted on monodisperse particle of 0.5 to 1 mm in diameter [50]. Unstable colloidal and predicates forms and aggregates for higher ratio values. Peptization is commonly carried out for these aggregates to achieve final size of usually less than 100 nm [59]. Higher pH of solution also contributes to increased particles size of the TiO_2 nanoparticles. Calcination process should be carefully determine as the phase transformation of the TiO_2 is highly influenced by the used temperature [60].

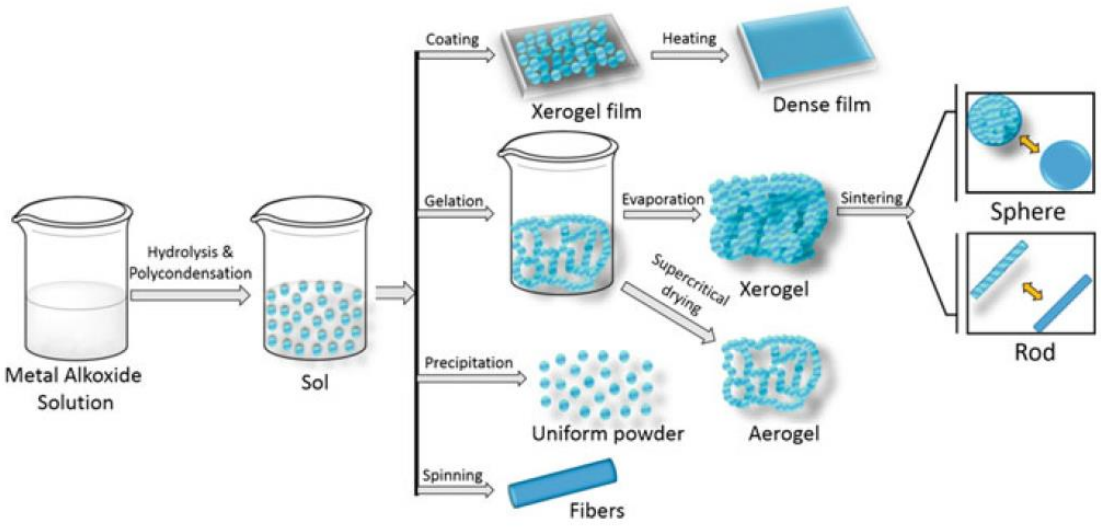

Figure 2.1: Schematic representation of the sol-gel processing by various synthesis route [61]

2.3.2 Thermal behavior

Thermal analysis is mainly a technique where the mass of a particular sample where evaluated against temperature. In turn, the information which can be gained is the physical or chemical changes of the product when subjected to heat [62]. Such technique is essential in synthesis process such as the sol-gel method to identify the reaction occurs at different temperatures. Suitable calcination temperature can also be determine from the thermal curve.

In synthesizing TiO_2 nanoparticles from solutions such as the sol-gel method, it is important to subsequently carry out heat treatment process on the obtained product. This is significant in order to attained crystalline structure which in turn possessed the preferable properties of the TiO_2 nanoparticles [63]. However, parameters and condition to attain optimum must be first determined. Thus, the thermal behavior obtained by the thermogravimetric analysis (TGA) is preliminary

investigated. In most cases, researchers utilized the maximum range of 30 to 900 °C when analyzing the synthesized TiO_2 nanoparticles [64, 65]. Additionally, both normal and inert gas atmosphere had been used during the procedures [66, 67].

For example, Guo et al. [64] studied the thermal behavior of the TiO_2 nanoparticles synthesized with different NH_4Cl ratio, R. The TiO_2 were heated up to 800 °C in air atmosphere for the thermal analysis. Upon reaching to temperature of ~452 °C, the weight loss recorded tend to stabilized reflecting the absence of further physical or chemical changes (Figure 2.2). The mass loss below such temperature were associated to the removal of the physically absorbed water and followed by the decomposition of the chemically bonded hydroxyl group [68]. Most importantly, this somehow portrays the optimum calcination temperature to attained well crystalline TiO_2 nanoparticles; which indeed fall within the range of 400- 450 °C [69, 70].

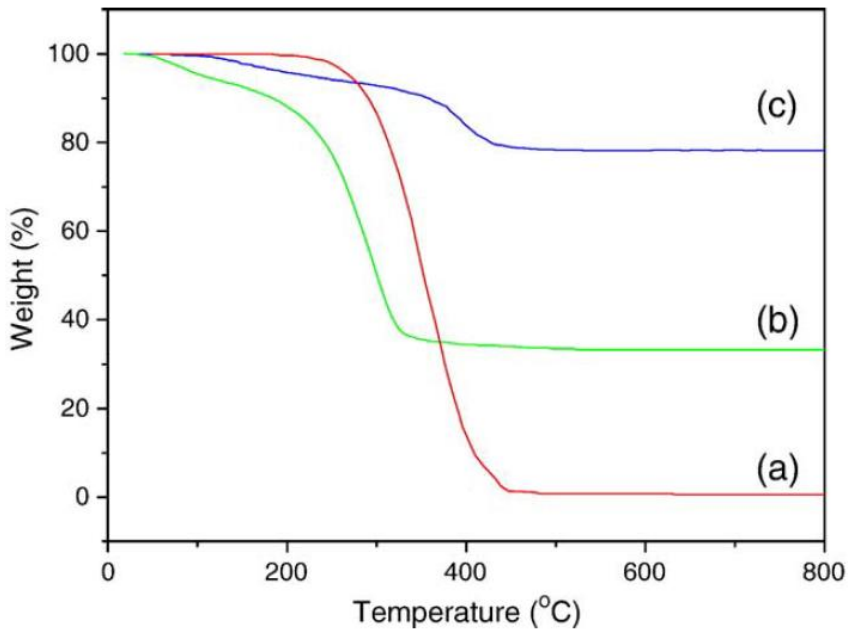

Figure 2.2: The TGA curves of the synthesized TiO_2 nanoparticles with different NH_4Cl ratio of (a) R = 1, (b) R = 2 and (c) R = 0 [64]

In investigating the effects of additives and surfactants (such as the usage of acids), thermal analysis conducted in gas flow is much preferable [66]. In this case, the highest weight loss was attained by TiO_2 synthesized at 25 °C with 9 ml acetic acid (TN9-25) (Figure 2.3). While the highest was attained by TiO_2 with no acetic acid synthesized at 80 °C (TN0-80). The large portions of the mass loss in the first region mainly explain the evaporation of physically absorbed solvent [71]. Upon the degradation of the non-reactive titanium precursor and the elimination of the hydroxyl groups), crystalline TiO_2 again was observed to be possibly obtained after heat treatment at 400 °C and above due to the absence of any further loss in mass [72, 73].

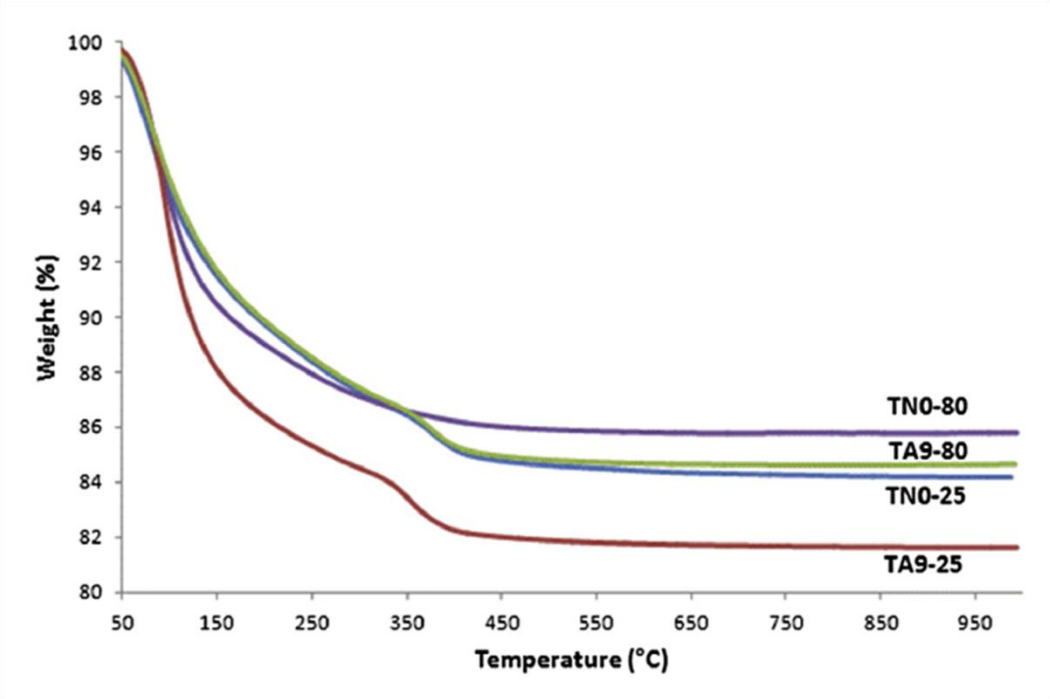

Figure 2.3: The TGA curves for the sol-gel synthesized TiO_2 nanoparticles with different amount of added acetic acid [66]

2.3.3 Phase and structural analysis

The phase and structural analysis is a significant characterization technique in characterizing sol-gel synthesized TiO_2 nanoparticles. The means of X-ray diffraction (XRD) were been utilize to qualitatively identify the phases obtained by referring to the XRD databases [74].

The information that can be obtained includes the phase analysis and identification; where presence of either pure or mixtures of anatase, rutile and brookite phases can be determined according to the peaks position. Plus, structural parameters were also extracted from the database. Such data can be further analyze through the Rietveld refinement, yielding more information including crystallite size determination, phase quantification and fitting parameters.

Physically, the fine powder form of the TiO_2 nanoparticles provides relatively easy sample handling and preparation; ensuring smooth and flat surface. This is important as sample displacement is the main factor contributing to errors in the analysis [75]. The dominant TiO_2 diffraction peaks mainly lies between the angle of $2\theta = 25° - 30°$. Thus, Bragg angle range of $2\theta = 20° - 80°$ was practically applied in analyzing the TiO_2 nanoparticles [76, 77]. Due to increase in crystallinity, TiO_2 nanoparticles subjected to calcination were commonly associated to higher peak intensity counts [78]. In addition, the lattice plane corresponding to the particular peak mainly reflects the preferable growth orientation of the TiO_2 nanoparticles crystal [74, 79, 80].

Comparison of the XRD patterns by Li et al. [81] for TiO_2 nanoparticles synthesized with different protonating agents clearly portrayed that the surface modification on the sol colloids significantly resulted in different mixtures of the

TiO_2 polymorphs **(**Figure 2.4**)**. Phase analysis identified the detected peaks to the anatase TiO_2 (JCPDS 21-1272) [82, 83]. Additionally, absence of other TiO_2 polymorph phases with the usage of milder acetic acid during the synthesis was mainly common due to the less availability of the hydroxyl group [84]. In different view, this clearly support that the phase preferences were highly dependent on the preliminary stages of the sol-gel synthesis. As such destabilization induced by either physically or chemically absorbed solvent could favorably encourage the anatase to rutile transformation [85].

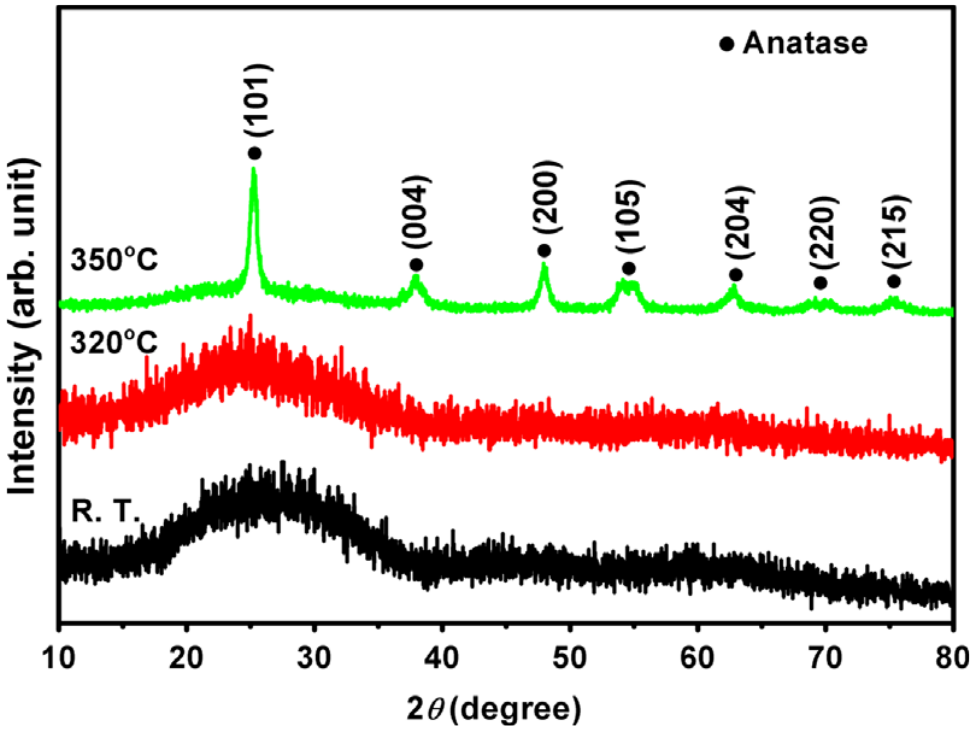

Figure 2.4: X-ray diffraction patterns of the as-dried TiO_2 precursor samples calcined at different temperatures in air for 2h [81]

In another example, the phase analysis confirmed that single pure anatase phase (JCPDS File No. 21-1272) had been successfully attained with varying amount of ferric nitrate (0 – 1 mole %) [76]. Structural parameters (a = 3.779 Å, b =3.779 Å, c = 9.493 Å) were also retrieved from the identification card. In this case, due to the absence of any secondary phases from the XRD pattern, it can be concluded that the added Fe^{3}+ had successfully favors the formation of pure anatase TiO_2 nanoparticles (Figure 2.5). This explains the influence of promoting surface hydroxyl on the acquisition of pure anatase TiO_2 phases [86, 87]. Interestingly, the influence of physically induced interaction (centrifuge/ storage) should receive similar attention in investigating sol-gel synthesized TiO_2 nanoparticles.

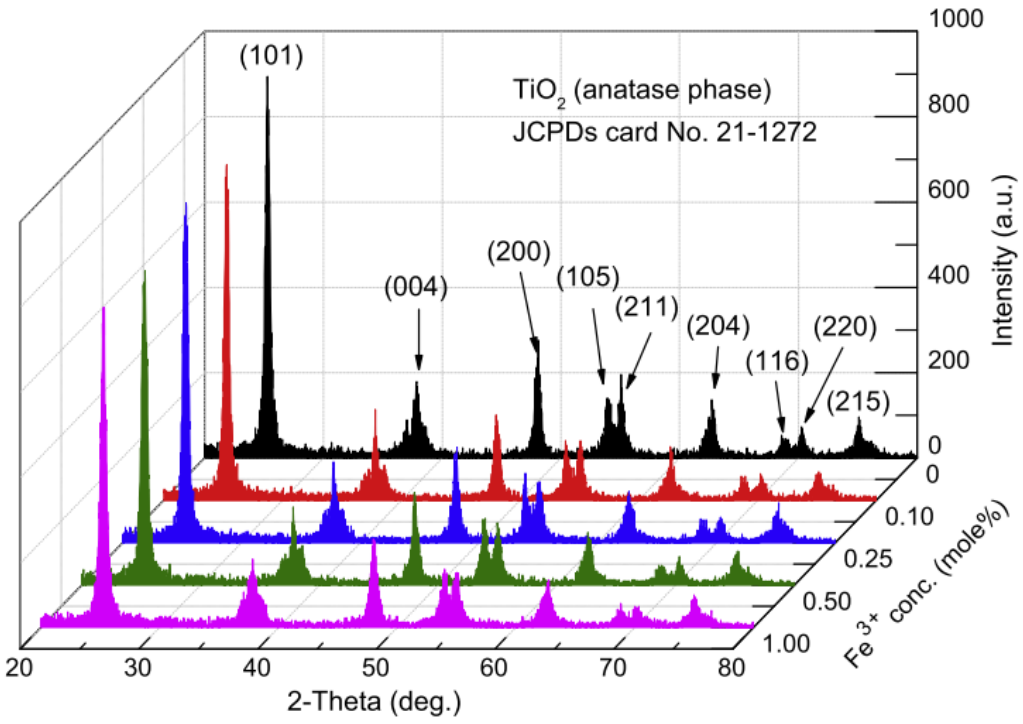

Figure 2.5: The XRD patterns of calcined TiO_2-based photocatalysts with different Fe^{3+} doping levels [76]

2.3.4 Rietveld refinement

The Rietveld analysis is a technique which involves the fitting of a simulated XRD model onto the obtained pattern from the XRD analysis; reflecting the reliability of the corresponding XRD pattern. The techniques were favorably practiced to further characterize the synthesized TiO_2 nanoparticles, providing in-depth evaluation of the phases and the fitting parameters.

Corresponding to the analysis provided by the XRD, further interpretation on the XRD curve through Rietveld refinement provides valuable information. Through the least square method, the software minimize the difference between the patterns yielding quantitative data such as phase percentage and the crystallite sizes [88]. Additionally, the fitting parameters evaluation (R profile (R_{wp}), R expected (R_{exp}) and the goodness of fit (GOF)) can also be obtained.

The Reitveld refinement utilizes the data obtained from the XRD. Thus, factors which affect the XRD analysis are also responsible in determining the accuracy of the Reitveld refinement. Phase quantification from the Rietveld analysis was attributed to the intensities of the diffraction peaks, determining the phase percentages of the TiO_2 anatase, rutile or brookite. Additionally, increment on the full width at half maximum (FWHM) of the TiO_2 polymorphs peaks reduces the resultant crystallite sizes of these phases [89]. The fitting between the optimized model generated from the observed and computed intensities mainly reflects the reliability of the synthesis process used [88]. The values vary accordingly to the different sol-gel approach used in synthesizing the TiO_2 nanoparticles; GOF ranges from 1.0 – 2.0 were obtained for the anatase TiO_2 attributed to different heat treatments [90, 91].

An example can be observed from the Rietveld refinements conducted on different TiO_2 nanoparticles synthesized with varying ratio of precursor to solvent during the sol-gel process [92]. Eventually, the fitted curves were evaluated to show no large differences among the samples (Figure 2.6). In addition, anatase lattice parameters were quite similar in sample 2 and 3, whereas the content of the secondary brookite was much larger for sample 3 (Table 2.1). This alternately reflects that the altering on the precursor ratio promote only slight deviation on the resultant structural properties of the TiO_2 nanoparticles.

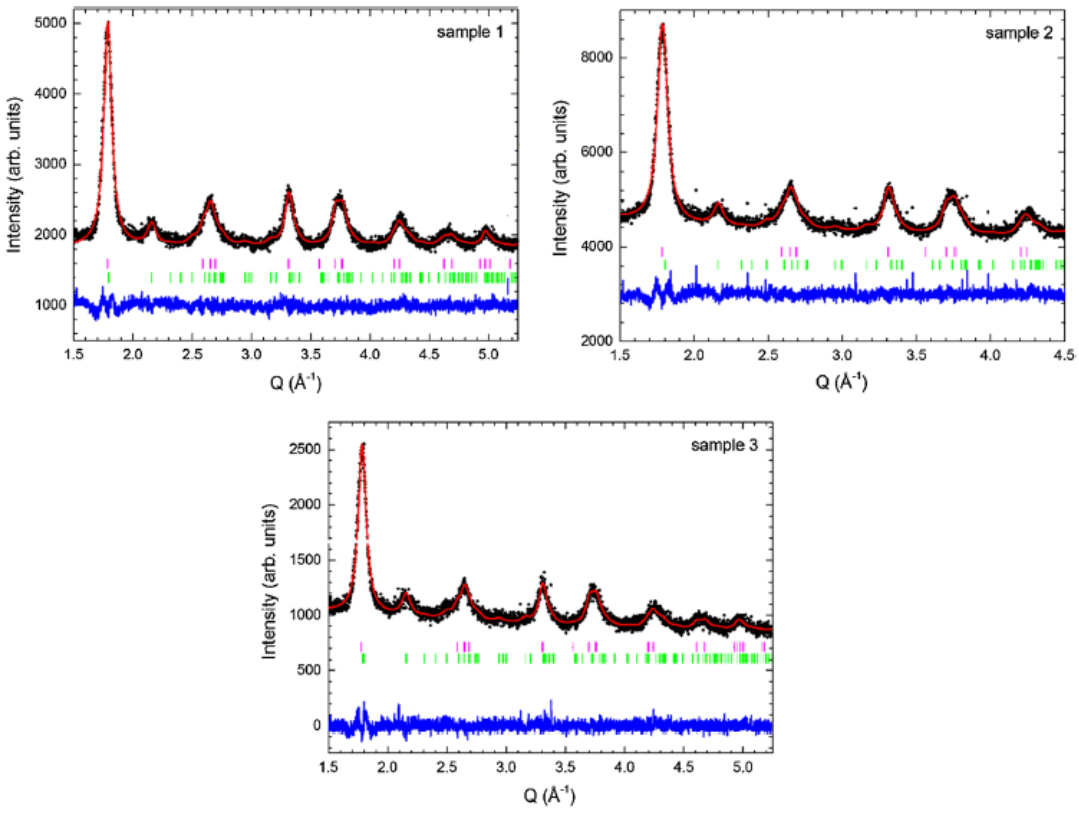

Figure 2.6: The refined XRD patterns of the TiO_2 nanoparticles synthesized with varying ratio of precursor to solvent [92]

Table 2.1: Structural and microstructural data obtained after Rietveld refinement for TiO_2 nanoparticles synthesized with varying precursor to solvent ratio [92]

	Sample 1	Sample 2	Sample 3
a (A°)	3.7946 (1)	3.8002 (1)	3.8026 (2)
c (A°)	9.4772 (4)	9.4918 (3)	9.4937 (2)
Brookite (wt%)	26.5 (1)	27.8 (1)	35.5 (2)
Rwp (%)	2.77	1.75	3.86

In the case of Fe doped TiO_2 nanoparticles, first, the best fits between calculated (solid line) and observed (dotted line) were mainly observed to locate any deviation/differences among the two [93]. For instance, by inspecting the difference between the curves, a good agreement between observed and calculated data of the TiO_2 nanoparticles were mainly presented (Figure 2.7). The phase of the anatase and brookite were also quantitatively presented for all of the samples. In addition, the fitting parameters generated (GOF and R_{wp}) also reflect the good reliability of the curves for the anatase phase in comparison to the rutile (Table 2.2). The increment of lattice parameters due to the Fe doping was mainly attributed to the Fe cation action, plus with the presence of polyethylene glycol [94]. This further represent the differences on the refinement parameters between the synthesized S1 (no Fe doping) and S2 (with Fe doping) TiO_2 nanoparticles.

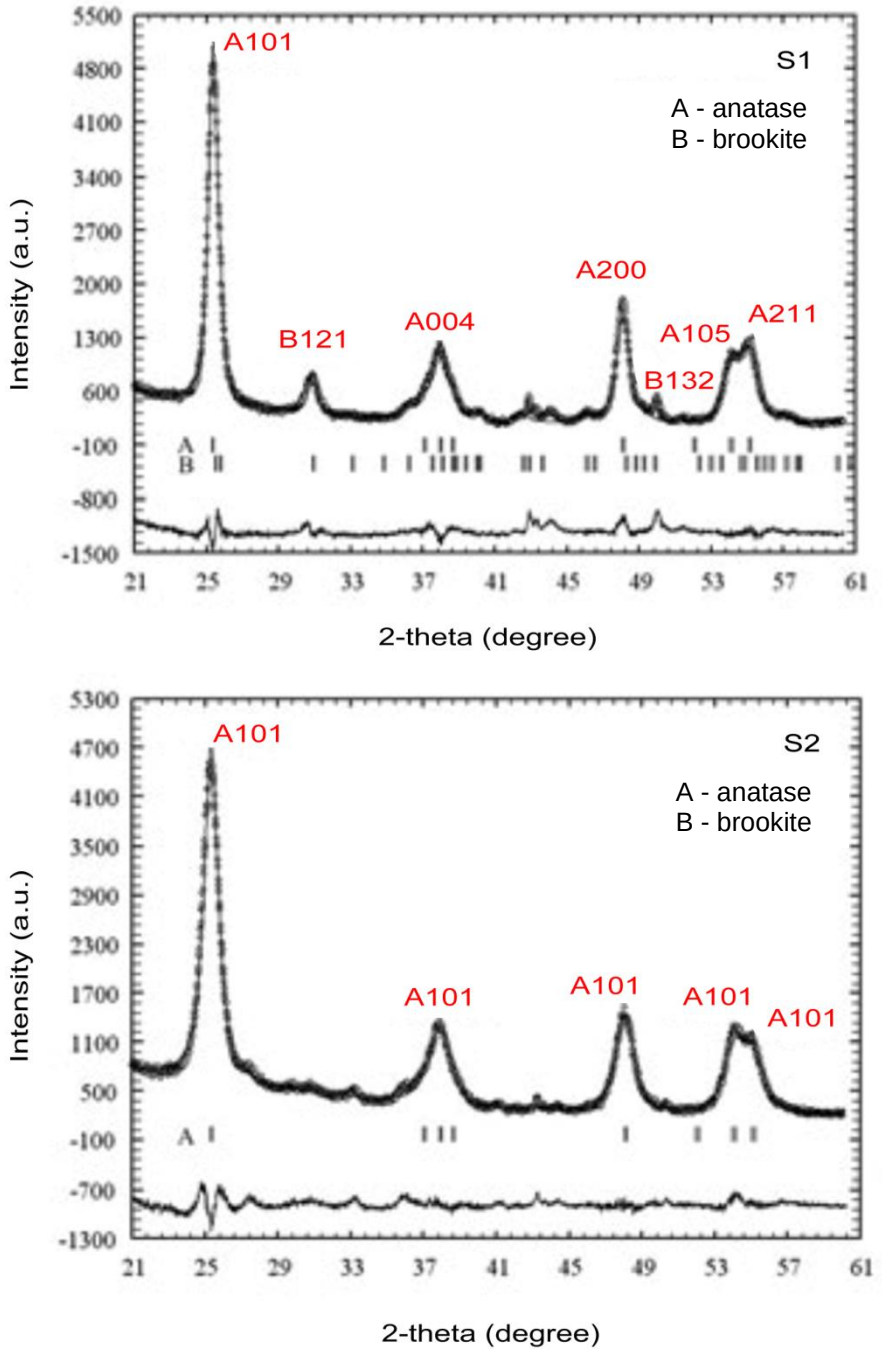

Figure 2.7: The fitted profiles of calcined TiO_2-based photocatalysts with different Fe doping concentration [93]

Table 2.2: Crystallographic data and results of Rietveld refinement of nanocrystalline TiO_2 synthesized different Fe^{3+} doping concentration [93]

Sample	S1	S2
Phase, Z	TiO_2, 4	TiO_2, 4
Lattice parameters (nm)	a=0.379(1), c=0.941(1)	a=0.385(1), c=0.946(3)
Cell volume (nm^3)	0.1353(4)	0.140(1)
Ti site	4 (b)	4 (b)
Position (x, y, z)	(0, 0.25, 0.375)	(0, 0.25, 0.375)
O site	8 (e)	8 (e)
Position (x, y, z)	(0, 0.25, z) z= 0.158(2)	(0, 0.25, z) z= 0.169(3)
	Phase composition	
Anatase (%)	74.5	100
Brookite (%)	25.5	0
Rwp (%)	2.94	17.3
GoF-index	0.9	0.7

2.3.5 Morphological and elemental analysis

Morphologies observation is an important qualitative characterization and were been conducted from electron microscopy, commonly the FESEM [95] and HRTEM [96]. Selection on the characterization method usually depends on the samples suitability and resolution of the techniques. Method such as the FESEM and HRTEM offers higher versatility as both can be further exploits to compensate additional analysis such as the elemental analysis.

In FESEM imaging, the secondary electron (SE) mode was more preferable compared to backscattered electron (BSE) mode; SE mode allow more detailed surface images of the TiO_2 nanoparticles which is more significant compared to the BSE mode [95]. This is significant in allowing better interpretation on the micrographs as the TiO_2 nanoparticles are commonly subjected to agglomerations.

The observation on the morphology of the TiO_2 nanoparticles commonly requires magnification up to 30000x [97]. However, higher magnification up to 100,000x had also been reported in characterizing the surface morphology of the TiO_2 nanoparticles [95]. These mainly depend on the condition of the TiO_2 nanoparticles prior to characterization. Dry TiO_2 nanoparticles resulted from calcination allows higher magnification observation compared to un-calcined nanoparticles. Coatings with conductive metal such as gold are required prior to imaging. In addition, less crystalline TiO_2 nanoparticles were subjected to higher charging effects during the observation process.

The SE images obtained by Ning et al. [95] shows significant differences on the morphology of the rutile and anatase TiO_2 nanoparticles **(**Figure 2.8**)**. The shapes and surface morphology for both TiO_2 nanoparticles were been obtained with 100,000x magnification. Due to the sufficient magnification, the distribution of the primary particles and the agglomeration of the particles can be clearly observed in the micrographs. Calcination of these TiO_2 nanoparticles mainly contribute to these high magnification images which provide easier interpretation in analyzing the TiO_2 nanoparticles.

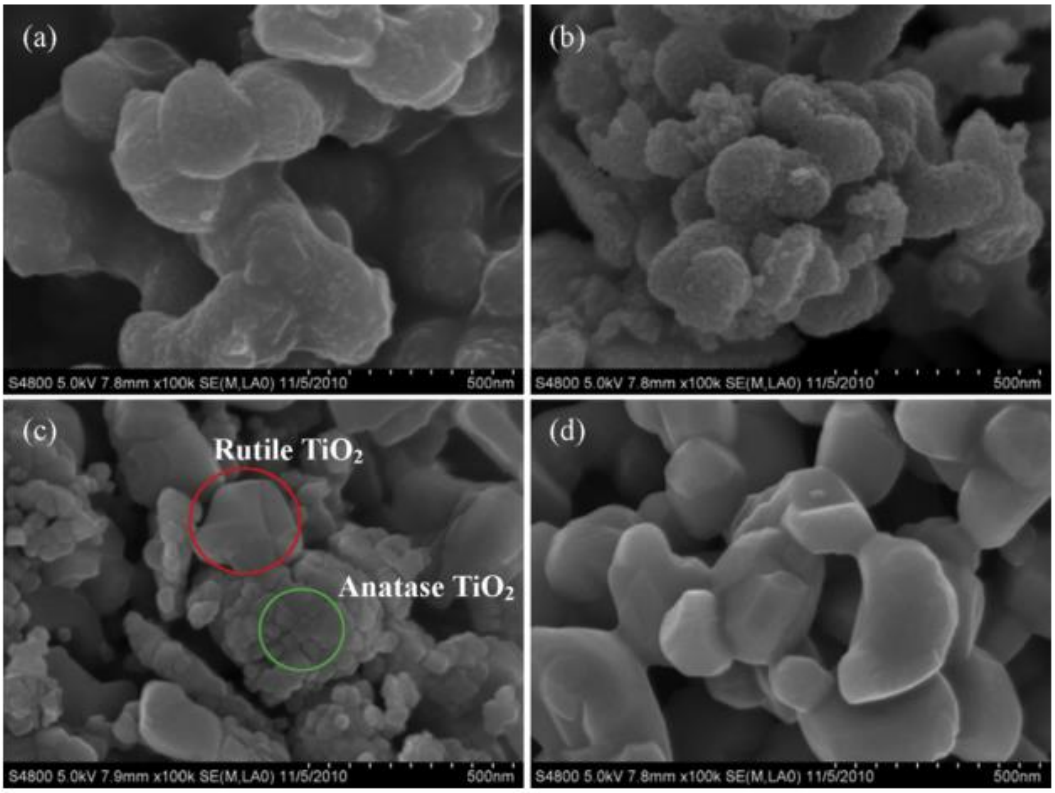

Figure 2.8: SEM images of amorphous TiO_2 after heat treatment at different temperatures: (a) without heat treatment; (b) 450°C; (c) 700°C and (d) 900°C [95]

Apart from that, the influence of calcination on the size of the synthesized TiO2 nanoparticles were clearly differentiated from the SEM images [98]. The heat treatment carried at varying temperatures (600 ◦C, 700 ◦C, 800 ◦C and 900 ◦C) induced favorable growth of the TiO_2 particle size (Figure 2.9). These increments are indeed logical due to the phase transformation of the anatase to larger rutile polymorphs at such high temperatures [99, 100]. Again, the morphological behaviors in term of the reduction on the particles agglomeration were also observable from the obtained micrographs.